https://doi.org/10.5194/egusphere-2026-6353
Preprint. Discussion started: 9 November 2026
© Author(s) 2026. CC BY 4.0 License.

Joint retrieval of atmospheric temperature and water vapor from AIRS thermal infrared and OCO-2 near-infrared measurements

Fredrick W. Irion[1], Robert R. Nelson[1], Christopher Hepplewhite[2], James McDuffie[1], Robert C. Wilson[1], Sun Wong[1]

[1]Jet Propulsion Laboratory, California Institute of Technology, Pasadena CA 91109, USA
[2]University of Maryland – Baltimore County, Baltimore MD 21250, USA

Correspondence to: Fredrick W. Irion (bill.irion@jpl.nasa.gov)

Abstract.

Combining thermal-infrared emission measurement with near-infrared absorption measurement can be a pathway to improved remote sensing of temperature and water vapor profiles from the surface to the upper troposphere. The addition of near-infrared radiance data to the thermal can significantly enhance the information content close to the surface in the planetary boundary layer, and is effective in clear or near-clear daytime conditions over land and ocean glint. A proof-of-concept study is presented using thermal-infrared Atmospheric Infrared Sounder (AIRS) radiances combined with near-coincident, near-infrared radiances from the Orbiting Carbon Observatory-2 (OCO-2) in a joint optimal estimation retrieval. Results indicate a significant increase in information content and reduced retrieval error for both temperature and water vapor between the surface and ~800 mb. Comparisons of retrieved profiles to coincident radiosondes show limited-to-no reduction in biases of temperature and water vapor over the forecast-derived a priori near the surface, indicating that improvements in the forward-modelling and/or retrieval algorithm are needed.

Copyright 2026 California Institute of Technology. Government sponsorship acknowledged.

1 Introduction

Earth's Planetary Boundary Layer (PBL) can be generally defined as the turbulent layer at Earth's surface; the vertical extent of which can vary from a few tens of meters to ~5 km, but is typically around 1 km. (See Sect. 2 of Teixeira et al., 2021.) With large variations geographically and temporally, the PBL is the transition region exchanging energy and water between Earth's surface and the free troposphere. People experience the weather in the PBL; global observation of its temperature, humidity and cloud structures, with increases over current measurement in both vertical and horizontal resolution, is necessary for needed improvement in weather, climate and air quality prediction.

Prospects for the development of remote sensing observing systems for the PBL were evaluated by Teixeira et al. in response to the National Academies of Sciences, Engineering and Medicine 2017-2027 Decadal Survey for Earth Science and Applications from Space (NASEM, 2018). Hyperspectral measurement of outgoing thermal-infrared (TIR) emission was

https://doi.org/10.5194/egusphere-2026-6353
Preprint. Discussion started: 9 November 2026
© Author(s) 2026. CC BY 4.0 License.

identified as a key technique (among several) to monitor and measure the PBL. However, as observed in Sect. 8.3.3 of Teixeira et al., reliable observation of the PBL by thermal emission instruments can be complicated not only by the presence of clouds, but also from often-present weak vertical thermal gradients in the PBL or low thermal contrasts between the surface and the lowermost atmosphere; these reduce or even eliminate the sensitivity and vertical resolution of TIR-retrieved water vapor. Figure 1 illustrates this problem using Global Navigation Satellite System Radio Occultation (GNSS-RO) measurement to the west of Baja California under clear conditions. The two water vapor profiles are similar, but the temperature gradient of the solid red observation line is nearly constant from the surface to ~850 mb – a condition where a TIR water retrieval would be expected to show poor sensitivity. Even with minimal cloud cover and good signal-to-noise, thermal-infrared measurement is hindered by low thermal gradients, or low altitude atmospheric inversions (which have a local zero in their gradients).

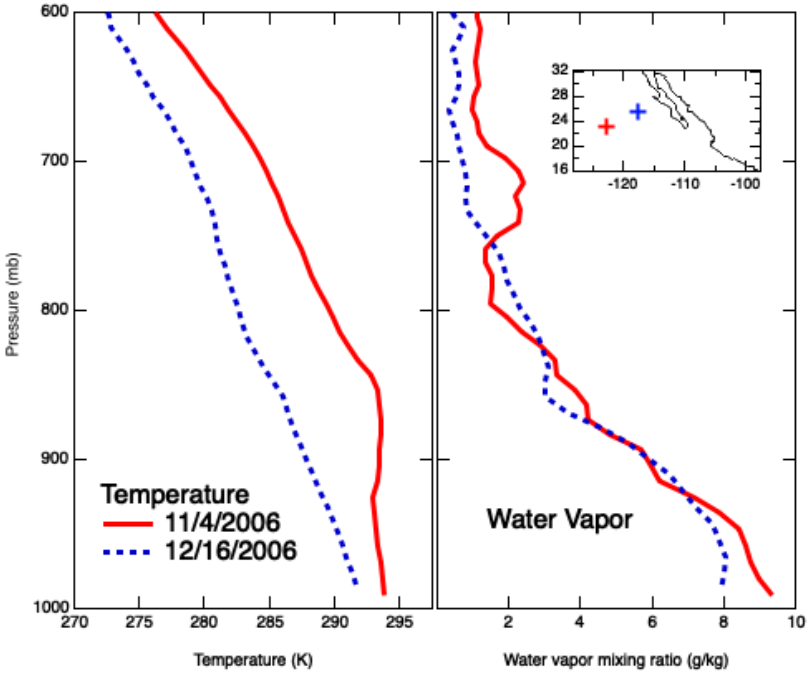


Figure 1: Sample daytime temperature and water vapor profiles in clear scenes from high vertical resolution GNSS-RO measurement, with inset map. Data courtesy of Qing Yue and Gerald Manipon (private communication, 2021).

In their discussion of the capabilities and limitations of thermal-infrared measurements, Teixeira et al. noted that extending the spectral range of observation to 1 μm to measure the total water column can provide a useful constraint to improve PBL retrieval. Here, we demonstrate that at least some of the limitations in PBL observation using TIR may be ameliorated by joint retrieval using near-infrared (NIR) spectra of reflected sunlight. Space-borne observations of NIR spectra have mostly been used for estimating column-average dry-air mole fractions of CO_2 (XCO_2) from the Greenhouse Gases Observing Satellite (GOSAT; Kuze et al, 2009), the Orbiting Carbon Observatory-2 (OCO-2; Crisp et al., 2008; Crisp, 2015), and on the International Space Station, the Orbiting Carbon Observatory-3 (OCO-3; Eldering et al., 2019; Basilio et al., 2019). However,

https://doi.org/10.5194/egusphere-2026-6353
Preprint. Discussion started: 9 November 2026
© Author(s) 2026. CC BY 4.0 License.

the NIR is also sensitive to temperature variation in CO_2 and water vapor near the surface under clear or near-clear conditions (Nelson et al., 2016). Put simply, as NIR observation of reflected sunlight is an absorption measurement, in specific spectral regions it is most sensitive where the bulk of atmospheric CO_2 and H_2O reside.

Profile retrieval using passive instruments on different platforms has been described for carbon monoxide using the Cross-track Infrared Sounder (CrIS) on the Suomi National Polar-orbiting Partnership (Suomi NPP) platform with either the Measurements of Pollution in the Troposphere (MOPITT) instrument on the EOS-Terra platform, or TROPOMI (Tropospheric Monitoring Instrument) on the Copernicus Sentinel-5 Precursor (S5P) satellite (Fu et al., 2016). Ozone was jointly retrieved using the Atmospheric Infrared Sounder on EOS-Aqua and the Ozone Monitoring Instrument (OMI) on EOS-Aura (Fu et al., 2018). Here, as a proof-of-concept for temperature and water vapor, we use existing programs-of-record of TIR measurement from AIRS (Aumann et al., 2003), and NIR measurement from OCO-2. As more fully discussed below, the NIR can "fill in the gap" during daytime and (near-)clear conditions where the TIR can lose sensitivity in the PBL. A joint retrieval of temperature and water vapor using both the TIR and NIR can thus provide continuous profiles from the surface to the upper troposphere. Both the AIRS and OCO-2 instruments were part of the "Afternoon Train" (L'Ecuyer and Jiang, 2010), a ~700 km sun-synchronous polar orbit, between the OCO-2 launch in July 2014, with OCO-2 ahead by 7-8 minutes, until AIRS began to free drift around January 2022 (due to exhaustion of fuel needed for orbital correction). As a gauge to evaluate any increase in retrieval information by adding NIR to TIR, we compare atmospheric retrievals using only AIRS spectra ("AIRS-only") and retrievals combining AIRS and OCO-2 spectra ("AIRS+OCO-2").

2. Instruments and co-location criteria

2.1 AIRS description

The Atmospheric Infrared Sounder (AIRS) instrument is an infrared grating spectrometer with 2378 channels ranging from 3.7 to 15.4 μm (including gaps) with resolving power $\lambda/\Delta\lambda = 1200$. (Aumann et al., 2003). In a "single-footprint" retrieval, it has a horizontal resolution of approximately 13.5 km at nadir view. Figure 2 illustrates a sample spectrum in brightness temperature. AIRS operated on-board the EOS-Aqua platform in the polar-orbiting, sun-synchronous Afternoon Train with an ascending equator-crossing time of 1:30 PM (before the free drift). Built to provide global measurements akin to radiosondes, AIRS data have improved weather prediction, and enhanced understanding of the atmospheric energy and water cycle (Chahine et al., 2006). AIRS has returned spectra in near-continual observation since September 2002.

https://doi.org/10.5194/egusphere-2026-6353
Preprint. Discussion started: 9 November 2026
© Author(s) 2026. CC BY 4.0 License.

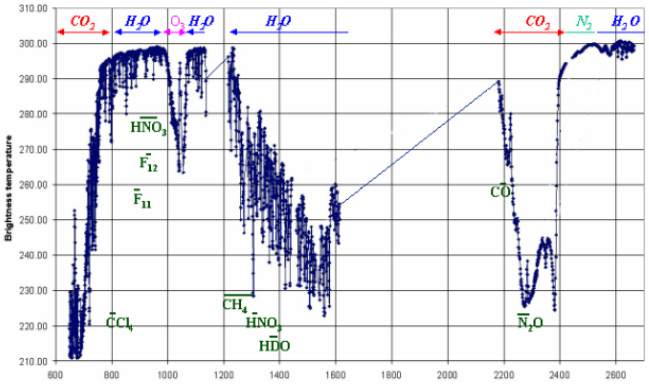


Figure 2: Sample clear AIRS spectrum with a 301K surface temperature (from Aumann et al., 2003).

2.2 OCO-2 description

OCO-2 is a grating spectrometer of resolving power >17,000 within three narrow spectral bands centered at 0.76, 1.6 and 2.0 μm. Using reflected sunlight in the near-infrared, OCO-2 was designed to measure XCO_2 in scenes sufficiently free from clouds and aerosol and with a nadir footprint of ~1.3 km x 2.3 km. OCO-2 has returned data since September 2014, and being also on the Afternoon Train, was about 7-8 minutes "ahead" of AIRS. The 0.76 μm bandpass of OCO-2 is primarily for sampling the O_2 A-band, which is used for determination of total airmass (and surface pressure), and detecting aerosol and cloud contamination. While CO_2 is the dominant absorption species in the 1.6 and 2.0 μm bandpasses of OCO-2, significant absorption lines by water vapor can be measured (Figure 3). Retrieved total water vapor columns from these lines compare well with validation data (Nelson et al., 2016).

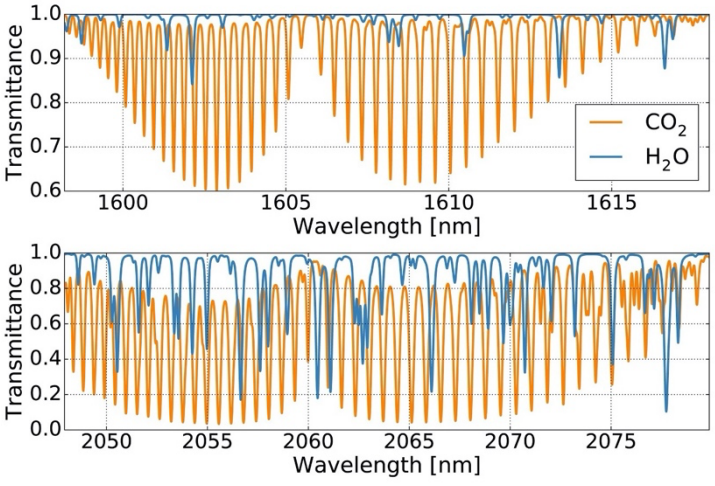


Figure 3: Sample calculation of CO_2 and H_2O transmittance in 1.6 μm and 2.0 μm bandpasses of OCO-2 (from Nelson et al., 2016).

https://doi.org/10.5194/egusphere-2026-6353
Preprint. Discussion started: 9 November 2026
© Author(s) 2026. CC BY 4.0 License.

2.3 Data sets and co-location criteria

As OCO-2 relies on reflected sunlight, only daytime observations for AIRS can be matched. (Note also that the NIR observation over ocean requires viewing the glint spot for sufficient signal. See Crisp et al., 2004). As noted, AIRS and OCO-2 are on different platforms in the same Afternoon Train orbit. We use location data from the instruments' Level 1b (radiance) files, and for a spatial co-location, the center of the OCO-2 footprint must be within a 5 km radius of the center of the AIRS footprint. To select OCO-2 observations that are of sufficiently good quality, we use Level 2 results from operational OCO-2 XCO_2 retrievals, which uses O_2 A-band channel radiances for surface pressure calculation. If the operational OCO-2 retrieval passed pre-processing "clear sky" criteria (Taylor et al., 2016) and met retrieval convergence criteria, it was used in matching to AIRS even if the retrieval result did not pass further strict XCO_2 OCO-2 quality control (as recorded by the "xco2_quality_flag.") Note that as the nadir footprint of AIRS is much larger than that of OCO-2, several OCO-2 observations can be made within an AIRS footprint. Within these criteria, approximately 50,000 to 60,000 matchups per day can be identified.

3. Retrieval, information content and quality control

3.1 Optimal Estimation Cost Function

For retrievals, we use the Joint Single Footprint Retrieval Algorithm (JoSFRA), which is also the basis for the optimal estimation "single-footprint" AIRS-only retrievals (Irion et al., 2018; 2025). Optimal estimation (Rodgers, 2000) minimizes a cost function defined as the difference between the observed and modelled radiances subject to a noise constraint and additional a priori constraints if the problem is ill-conditioned (e.g., Bowman et al., 2006):

$$\mathbf{C} = [\mathbf{y} - \mathbf{L}(\hat{\mathbf{x}}, \mathbf{b})]\mathbf{S}_{\varepsilon}^{-1}[\mathbf{y} - \mathbf{L}(\hat{\mathbf{x}}, \mathbf{b})]^{\mathbf{T}} + [\hat{\mathbf{x}} - \mathbf{x}_a]\mathbf{S}_{\mathbf{a}}^{-1}[\hat{\mathbf{x}} - \mathbf{x}_a]^{\mathbf{T}} \quad (1)$$

where $\mathbf{y}$ = observed radiance; $\mathbf{L}(\hat{\mathbf{x}})$ = computed radiance for the retrieval state vector $\hat{\mathbf{x}}$ and additional fixed variables $\mathbf{b}$ using forward model $\mathbf{L}$; $\mathbf{S}_{\varepsilon}^{-1}$ = inverse noise covariance matrix; $\mathbf{x}_a$ = *a priori* state vector (e.g., first guess profile(s)); and $\mathbf{S}_a^{-1}$ = inverse a priori constraint covariance matrix. The retrieval state vector, $\hat{\mathbf{x}}$, can include scalar and profile elements for several constituents impacting the modeled and observed spectra.

In this retrieval, the cost function, $\mathbf{C}$, is extended to include observed and modelled spectral data from both AIRS and OCO-2:

$$\begin{aligned}\mathbf{C} = {} & [\mathbf{y}_{\mathbf{AIRS}} - \mathbf{L}_{\mathbf{AIRS}}(\hat{\mathbf{x}}, \mathbf{b})]\mathbf{S}_{\varepsilon,\mathbf{AIRS}}^{-1}[\mathbf{y}_{\mathbf{AIRS}} - \mathbf{L}_{\mathbf{AIRS}}(\hat{\mathbf{x}}, \mathbf{b})]^{\mathbf{T}} \\ & + [\mathbf{y}_{\mathbf{OCO2}} - \mathbf{L}_{\mathbf{OCO2}}(\hat{\mathbf{x}}, \mathbf{b})]\mathbf{S}_{\varepsilon,\mathbf{OCO2}}^{-1}[\mathbf{y}_{\mathbf{OCO2}} - \mathbf{L}_{\mathbf{OCO2}}(\hat{\mathbf{x}}, \mathbf{b})]^{\mathbf{T}} \\ & + [\hat{\mathbf{x}} - \mathbf{x}_a]\mathbf{S}_a^{-1}[\hat{\mathbf{x}} - \mathbf{x}_a]^{\mathbf{T}} \quad (2)\end{aligned}$$

The calculation for both instruments uses different forward models, $\mathbf{L}_{\mathbf{AIRS}}$ and $\mathbf{L}_{\mathbf{OCO2}}$, but the same state vectors, $\hat{\mathbf{x}}$ and $\mathbf{x}_a$. (As discussed below, the OCO-2 forward model only uses the temperature and water vapor profiles from the state vector.) The

https://doi.org/10.5194/egusphere-2026-6353
Preprint. Discussion started: 9 November 2026
© Author(s) 2026. CC BY 4.0 License.

vertical layering of temperature and water vapor is kept the same in both forward models. Figure 4 shows a simplified block diagram of the retrieval components.

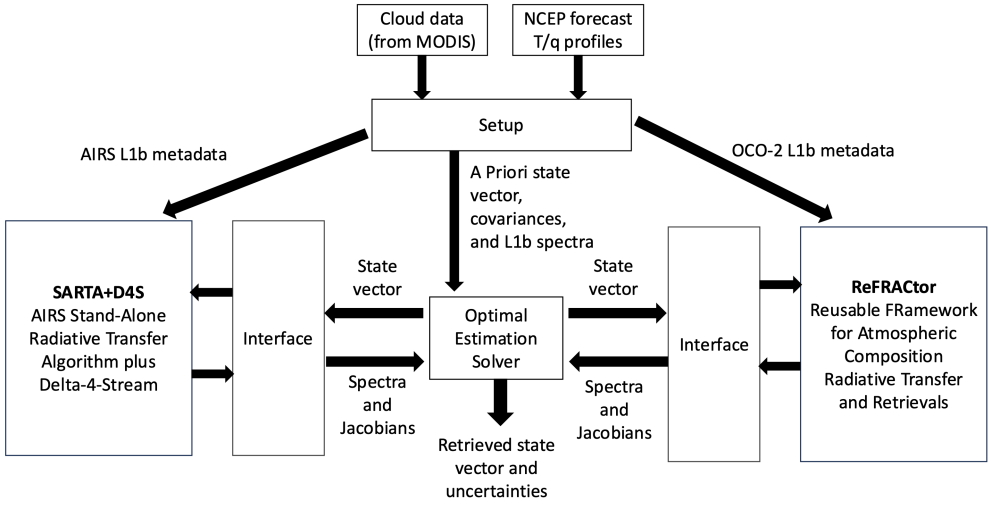


Figure 4: Simplified block diagram of retrieval setup.

3.2 A priori data

As AIRS and OCO-2 look at different parts of the electromagnetic spectrum, and have different-sized footprints, the AIRS and OCO-2 forward models only have the temperature, water vapor, and CO_2 profiles in common. Within the state vector, National Center for Environmental Prediction (NCEP) forecasts are temporally and spatially interpolated for a priori temperature and water vapor profiles, skin temperature, and for AIRS-only retrievals, surface pressure. For AIRS+OCO-2 retrievals, the posterior surface pressure from the operational XCO_2 retrievals is used. Cloud data from the Moderate Resolution Imaging Spectroradiometer (MODIS) on EOS-Aqua (Platnick et al., 2003, 2017) are used as cloud a priori for AIRS (but not OCO-2). These MODIS data are averaged over the AIRS footprint using the AIRS spatial response function (see Irion et al., 2018). For AIRS, we use the cloud effective emissivity rather than the daytime-only cloud optical depth, and calculate the initial cloud optical depth as

$$\tau_{cld} = -2. * \log_e(1. - \varepsilon_{cld}) \quad (3)$$

where τ_{cld} is the cloud optical depth, and ε_{cld} is weighted average of the MODIS cloud emissivity over the AIRS footprint. Cloud parameters are allowed to vary between iterations for fitting AIRS spectra (see Irion et al., 2025.)

Within the AIRS+OCO-2 retrievals, for the OCO-2 forward model, we use existing Level 2 results from OCO-2 operational XCO_2 retrievals (CO_2 profile, surface pressure, reflectivity, cloud and aerosol loading, and fluorescence over land) as fixed a

https://doi.org/10.5194/egusphere-2026-6353
Preprint. Discussion started: 9 November 2026
© Author(s) 2026. CC BY 4.0 License.

priori, but as indicated by Eq. 2, temperature and water vapor profiles are kept the same across the AIRS and OCO-2 forward models in each iteration of the retrieval. Note also that for AIRS+OCO-2 retrievals, the existing posterior OCO-2 L2 surface pressure is used as fixed a priori both for the AIRS and OCO-2 forward models. As mentioned, several OCO-2 footprints can fit within the field-of-view of AIRS; we assume that the temperature and water vapor are the same for both instrument observations, but cloud obscuration can be different.

Ocean emissivity for AIRS observations uses the NCEP Environmental Modeling Center (NCEP/EMC) Infrared Sea Surface Emissivity (IRSSE) formulae and coefficients (van Delst, 2003), calculated for channel frequency, view angle and wind speed, with the latter estimated from the NCEP forecast. These ocean emissivities are not modified in the retrieval.

For AIRS land observations, we start with monthly maps of land emissivity at "hinge" frequencies 699.3, 826.4, 925.9, 1075.2, 1204.8, 1315.7, and 1724.1 cm^{-1} gridded spatially by 0.05° (Seemann et al., 2008). These maps were for calendar years 2003 through 2014, and data were averaged for each grid point on a month-by-month basis, with variance calculated. The land emissivity for each AIRS retrieval channel was calculated by linear interpolation by wavelength (not frequency) between hinge points, with endpoints used when frequencies were out-of-range. (That is, the emissivity at 699.3 cm^{-1} was used for channels at lower frequencies.) To avoid unphysical values of emissivity in the forward model, we use the logistic function to restrict the emissivity to be between 0 and 1:

$$\varepsilon_{surf} = \frac{L}{1+\exp(-k[\xi-\xi^*])} \quad (4)$$

We select L = 1, k = 1 and $\xi^* = 5$. Thus, the "logistic parameter" function becomes:

$$\xi = 5 - ln\left(\frac{1}{\varepsilon_{surf}} - 1\right) \quad (5)$$

Within the retrieval, we solve for ξ, converting back to ε_{surf} via Eq. 4 when emissivity is input into the forward model. The value for ξ is initialized from the a priori ε_{surf}. The covariance for ξ is calculated from the variance of monthly emissivities at its grid point, and we assume no covariance between hinge points. Note that the retrieval need not use AIRS channels corresponding to the hinge points; the hinge point frequencies are just a basis on which to interpolate the emissivity to the retrieval channels.

3.3 Forward modelling and retrieval

To model AIRS spectra, we use the Standalone AIRS Radiative Transfer Algorithm + Delta-4-Stream (SARTA+D4S; Strow et al., 2003; Ou et al., 2013). This is adapted from what is used operationally by AIRS for "cloud-cleared" spectra (Susskind et al., 2003), but with additional D4S routines that calculate the effective cloud absorption given the cloud-top temperature,

https://doi.org/10.5194/egusphere-2026-6353
Preprint. Discussion started: 9 November 2026
© Author(s) 2026. CC BY 4.0 License.

effective cloud optical depth[1] and effective particle size for ice and water clouds. In contrast, the cloud and aerosol state vector elements within the OCO-2 retrieval are not retrieved but are instead fixed at the operational posterior result. The OCO-2 measurements used in this work are mostly free from cloud and aerosol contamination, but the state vector still includes scattering particles to account for thin cloud or aerosol layers. (See Nelson et al., 2019 for a complete description.)

OCO-2 spectra are modelled using the Reusable FRamework for Atmospheric Composition Radiative Transfer and Retrievals (ReFRACtor; McDuffie et al., 2020) implementing the Atmospheric Carbon Observations from Space (ACOS) retrieval algorithm described in O'Dell et al. (2012; 2018).

Early versions of the AIRS-only JoSFRA retrieval showed high biases of temperature and water vapor compared to ERA5 reanalysis when these were retrieved simultaneously using their stronger bands at frequencies less than 1650 cm^{-1}. These biases were ameliorated by retrieving in two steps. Temperature, surface temperature, AIRS clouds and (over land) surface emissivities are obtained first with AIRS channels selected for the surface and the 14 μm CO_2 band, while for OCO-2, the full 1.6 and 2.0 μm CO_2 bands are used (the 0.76 μm O_2 A-band is not used). In this first step, water vapor is retrieved as an "interferent" to improve spectral fitting, particularly for AIRS. In the second step, the water vapor a priori is reset to the NCEP forecast, and the AIRS channel selection switches to stronger water lines, mostly in the 6-8 μm region. The surface temperature, temperature profile, and cloud parameters retrieved in the first step are held fixed, and only water vapor is retrieved using

[1] The optical depth reported for AIRS, $\tau(c)$, is that at 0.55 μm. The optical depth, $\tau(\nu)$, at some wavenumber ν can be determined by the relationship $\tau(\nu) = \tau(c) \langle Q_{ext}(n) \rangle / 2$, where $\langle Q_{ext}(n) \rangle$ is the mean extinction efficiency for the spectral channel.

https://doi.org/10.5194/egusphere-2026-6353
Preprint. Discussion started: 9 November 2026
© Author(s) 2026. CC BY 4.0 License.

AIRS and the OCO-2 1.6 and 2.0 μm bands. Channel selection for AIRS is listed in Table 1. A priori covariances are listed in Table 2.

Table 1: AIRS retrieval channel frequencies used for Step One and Step Two

Step One channel frequencies (cm^{-1}) (for profile temperature, skin temperature and clouds)

662.02	670.06	689.76	698.82	708.70	719.17	740.03	773.28	839.92	1128.50
664.51	670.57	691.12	699.10	709.56	719.46	746.01	776.36	847.14	1129.04
666.26	672.10	691.39	699.38	711.00	719.76	747.60	778.08	849.57	1129.58
666.77	673.64	692.75	699.66	711.29	720.94	749.20	779.11	880.40	1130.12
667.27	675.19	693.02	700.77	712.74	721.54	750.48	790.33	917.30	1130.66
667.78	676.75	694.12	701.05	714.19	721.83	752.09	793.89	937.90	1231.33
668.28	677.01	694.40	702.74	714.48	723.03	753.38	798.92	1125.27	1231.85
668.54	678.31	694.67	703.87	715.94	723.32	753.70	801.10	1125.81	1232.37
668.79	678.57	695.77	704.43	717.99	724.52	755.00	803.65	1126.35	
669.04	681.46	696.05	706.13	718.28	726.32	755.32	804.75	1126.89	
669.55	681.72	697.43	706.99	718.58	734.15	758.26	811.79	1127.42	
669.81	689.49	697.71	707.84	718.87	738.48	769.89	820.84	1127.96	

Step Two channel frequencies (cm^{-1}) (for profile water vapor)

753.70	803.65	1324.97	1392.15	1423.75	1465.75	1493.21	1525.68	1569.29	1605.05
755.00	839.92	1367.25	1394.36	1427.22	1468.82	1498.96	1541.77	1572.09	
768.88	849.57	1367.78	1397.13	1430.13	1471.91	1500.88	1544.48	1576.32	
776.36	1121.00	1376.88	1399.35	1430.71	1475.00	1502.16	1547.20	1586.26	
778.08	1135.55	1379.58	1404.95	1432.47	1476.24	1513.83	1551.30	1589.84	
779.11	1218.49	1381.21	1407.77	1436.57	1479.36	1517.10	1554.04	1592.72	
793.89	1225.13	1384.47	1410.59	1441.88	1481.23	1519.07	1556.10	1593.44	
795.68	1310.18	1387.75	1419.15	1462.09	1483.74	1521.05	1560.24	1598.50	
798.92	1315.47	1389.39	1422.02	1465.14	1490.67	1524.35	1563.02	1603.59	

Table 2: A priori covariances used for retrievals

Constituent	sqrt(covariance) along diagonal	Covariance off-diagonal length scale (km)
Temperature profile (T_{atm})	1K from surface to 50 mb, then increasing to 15K at 10 mb and pressures below.	0.5
H_2O	$\log_e(1.4)$ from surface to 100 mb, then decreasing to $\log_e(1.01)$ at 50 mb and below.	0.5
Surface temperature (T_{sur})	2K	Not applicable
Cloud-top temperature	2K	Not applicable
Cloud optical depth	$\log_e(2)$	Not applicable
Cloud effective radius	$\log_e(2)$	Not applicable
Land emissivity	Varies (see text)	Not applicable

https://doi.org/10.5194/egusphere-2026-6353
Preprint. Discussion started: 9 November 2026
© Author(s) 2026. CC BY 4.0 License.

3.4 Averaging kernels and error estimation

Following Rodgers (2000), the Jacobian is the matrix of derivatives of the outgoing radiance to changes in each element of the state vector:

$$\mathbf{K_x} = \frac{\partial \mathbf{F}(\hat{\mathbf{x}},\mathbf{b})}{\partial \mathbf{x}} \tag{6}$$

The gain is a measure of the sensitivity of the retrieval to changes in the radiance:

$$\mathbf{G_x} = \frac{\partial \hat{\mathbf{x}}}{\partial \mathbf{F}} = (\mathbf{K_x^T S_\varepsilon^{-1} K_x} + \mathbf{S}_a^{-1})^{-1}\mathbf{K_x^T S_\varepsilon^{-1}} \tag{7}$$

The averaging kernel, **A**, is the gain multiplied by the Jacobian, and is a measure of the sensitivity of the retrieved state vector, $\hat{\mathbf{x}}$, to the true state vector, **x**:

$$\mathbf{A} = \frac{\partial \hat{\mathbf{x}}}{\partial \mathbf{x}} = \frac{\partial \hat{\mathbf{x}}}{\partial \mathbf{F}}\frac{\partial \mathbf{F}}{\partial \mathbf{x}} = \mathbf{G_x K_x} = (\mathbf{K_x^T S_\varepsilon^{-1} K_x} + \mathbf{S}_a^{-1})^{-1}\mathbf{K_x^T S_\varepsilon^{-1} K_x} \tag{8}$$

This is an n x n square matrix, where n is the number of elements in the state vector. The averaging kernel is useful in that it describes the sensitivity of one element of the retrieval state vector to a change in another element of the true state vector, that is,

$$A_{i,j} = \frac{\partial \hat{x}_{i,j}}{\partial x_{i,j}} \tag{9}$$

Figure 5 compares the rows of sample temperature and water vapor averaging kernels by AIRS-only and AIRS+OCO-2 observation. While the averaging kernels for both AIRS-only and AIRS+OCO-2 are mostly similar at pressures below ~700 mb, the addition of OCO-2 significantly improves sensitivity to both temperature and water vapor at pressures greater than 800 mb.

https://doi.org/10.5194/egusphere-2026-6353
Preprint. Discussion started: 9 November 2026
© Author(s) 2026. CC BY 4.0 License.

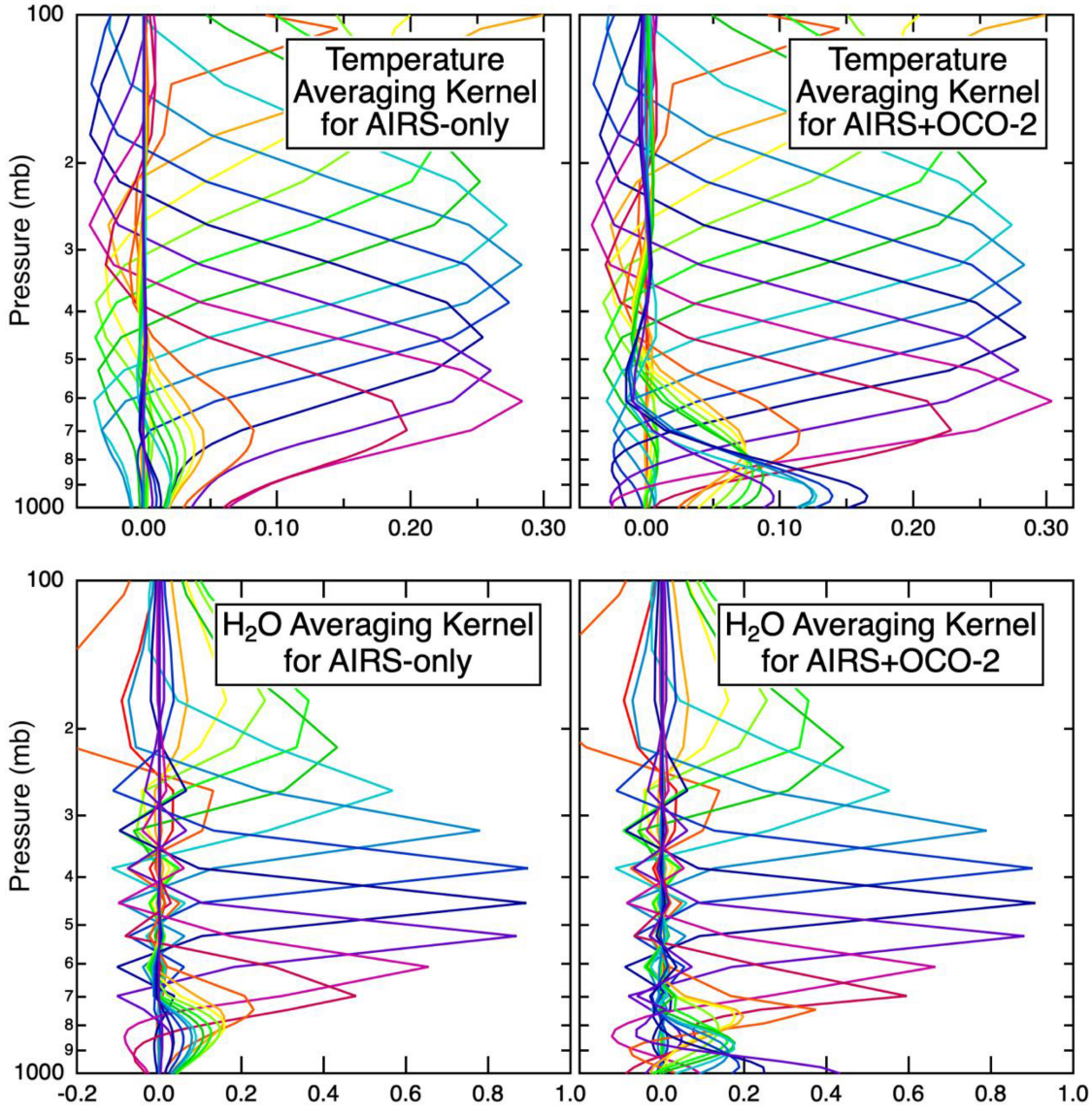


Figure 5: Rows of sample averaging kernels from AIRS-only and AIRS+OCO-2 temperature and water vapor retrieval. Retrievals were made for near-coincident oceanic AIRS and OCO-2 observations at 0.8°S and 36.7°W, on July 11, 2017.

The averaging kernel can be used to indicate the smoothing error, which is the uncertainty in the fine structure of the measurement due to limitations in the vertical resolution. (See Sects. 3.4 and 4.1 of Rodgers, 2000.)

$$\mathbf{S}_\mathrm{s} = (\mathbf{A} - \mathbf{I}_\mathrm{n})\mathbf{S}_a(\mathbf{A} - \mathbf{I}_\mathrm{n})^T \quad (10)$$

The retrieval noise covariance is a measure of error caused by instrument noise:

$$\mathbf{S}_\mathrm{m} = \mathbf{G}_\mathrm{x}\mathbf{S}_\mathbf{e}\mathbf{G}_\mathrm{x}^\mathrm{T} \quad (11)$$

https://doi.org/10.5194/egusphere-2026-6353
Preprint. Discussion started: 9 November 2026
© Author(s) 2026. CC BY 4.0 License.

Equations (8) and (9) can be combined (with substitutions) to provide the maximum a posteriori solution covariance:

$$\hat{\mathbf{S}} = (\mathbf{K}_\mathbf{x}^T \mathbf{S}_\boldsymbol{\varepsilon}^{-1} \mathbf{K}_\mathbf{x} + \mathbf{S}_a^{-1})^{-1} \quad (12)$$

The square roots of the diagonal of $\hat{\mathbf{S}}$ are reported as the posterior error. Note that this does not include systematic error (e.g., spectral error, or biases in the forward models) or uncertainties in a priori parameters not retrieved. Also, as the a priori covariances are ad hoc, the resulting random error should be treated with caution. However, Eq. (12) does allow comparison of random posterior error at different pressures and between AIRS-only and AIRS+OCO-2 retrievals, as will be shown below.

3.5 Reduced chi square fitting parameter

We use a reduced chi square fitting parameter, χ^2, as a goodness-of-fit statistic of how well a modelled spectrum is fitted within the bounds of the radiance error:

$$\chi^2 = \frac{1}{N} \sum_{i=1}^{N} \left(\frac{y_i - [\mathbf{L}(\hat{\mathbf{x}}, \mathbf{b})]_i}{\varepsilon_i} \right) \quad (13)$$

where N is the number of channels and ε_i is the radiance error in channel *i*. A $\chi^2 \gg 1$ generally indicates a poor spectral fit. While the χ^2 does not enter into the uncertainty calculation, it is used in quality control as described below.

3.6 Quality control (QC) filtering

To pass quality control, retrievals had to:

1. Converge within a maximum number of iterations. This was to avoid wasting computer time on non-convergent retrievals. (See Irion et al., 2018, for convergence criteria.)
2. Produce a surface temperature averaging kernel > 0.6 in step one. Note that the surface temperature is used in the AIRS forward model, and not in the OCO-2 forward model. It was noted in Irion et al. (2018) that AIRS retrievals below moderate to thick clouds could produce unphysically high values of relative humidity, due to limitations in the forward modelling of clouds. However, this effect was significantly less when AIRS would good sensitivity to the surface, which was determined from the surface temperature averaging kernel. Noting that AIRS has a larger footprint than OCO-2, this was to avoid situations where OCO-2 found a clear hole within a cloudy AIRS scene where the AIRS-part of the retrieval could induce an erroneous result in the PBL.
3. Produce a reduced chi-squared fitting, $\chi^2 < 3$ for both the step one temperature retrieval and the step two water vapor retrieval.

4. Results

We retrieve and compare results for AIRS-only observations and AIRS+OCO-2 joint observations. For a test day, we (arbitrarily) selected July 11, 2017. Noting that the OCO-2 forward model was originally developed for the exacting sub-part-per-million precision needed for XCO_2 (e.g., Miller et al., 2007), the forward modelling of OCO-2 CO_2 bands was slow

https://doi.org/10.5194/egusphere-2026-6353
Preprint. Discussion started: 9 November 2026
© Author(s) 2026. CC BY 4.0 License.

compared to AIRS. (Most of this time increase was from OCO-2 calculation of cloud and aerosol scattering). While an AIRS-only retrieval on a single footprint might take 10 to 20 seconds on one processor, an AIRS+OCO-2 retrieval might take 15 to 20 minutes. Thus, retrievals were attempted for all AIRS-only observations matched to an OCO-2 observation, but due to computer resource limitations, we only attempted retrievals for about 10% of the available AIRS+OCO-2 matchups for this day.

Figure 6 shows observation locations for 1943 QC-passed retrievals from AIRS-only observations, and 1728 QC-passed retrievals from AIRS+OCO-2 matched observations. About 90% of AIRS-only attempts passed QC, while only 35% of AIRS+OCO-2 attempts did so, mainly because most of the latter retrievals had $\chi^2 > 3$. Figure 7 compares AIRS-only and AIRS+OCO-2 temperature retrievals and calculated random error as a function of latitude at 607, 790, and 972 mb. To first order, the temperatures are consistent across the two sets. Figure 8 shows the 1σ posterior error of temperature as a function of pressure for both AIRS-only and AIRS+OCO-2. Again, noting that the a priori covariances are ad hoc, the calculated posterior error is substantially reduced at the lower altitudes because of the additional information that is provided by the OCO–2 NIR spectra.

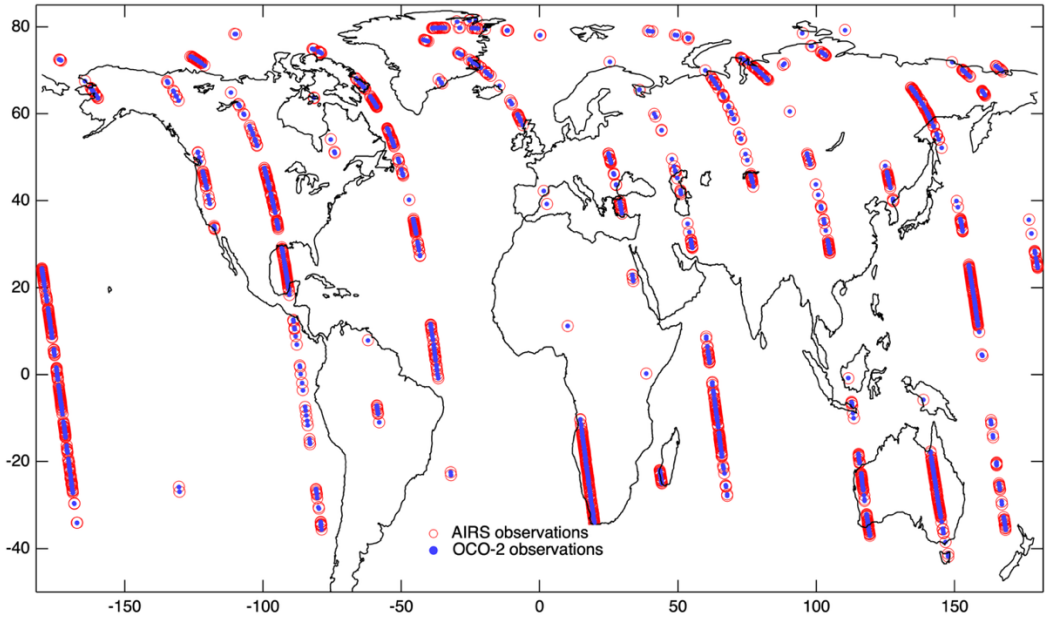


Figure 6: Locations of AIRS-only and AIRS+OCO-2 observations retrieved for July 11, 2017. Circles and dots are not scaled to footprint sizes.

https://doi.org/10.5194/egusphere-2026-6353
Preprint. Discussion started: 9 November 2026
© Author(s) 2026. CC BY 4.0 License.

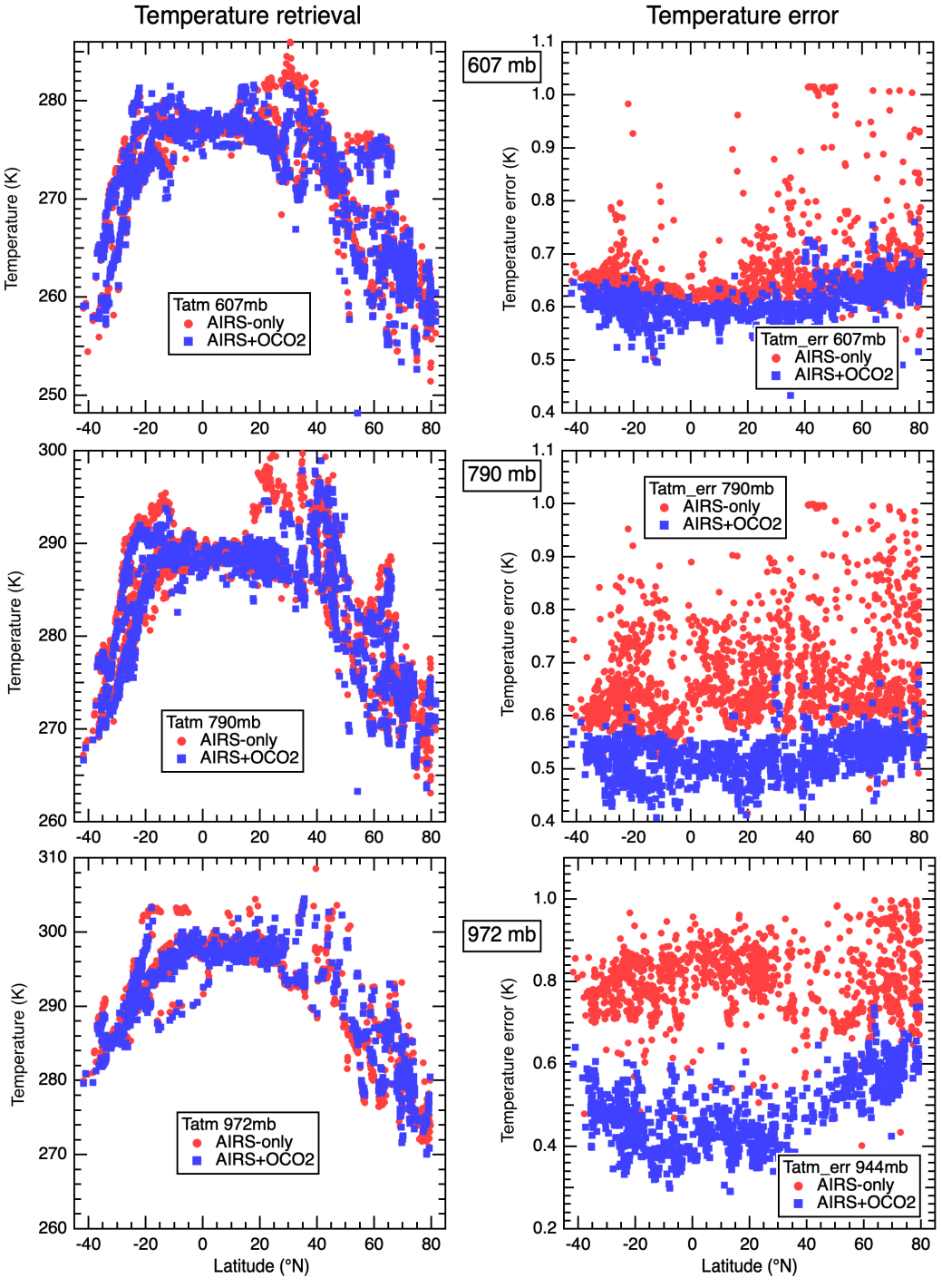


Figure 7: Latitudinal comparison of AIRS-only (red dots) and AIRS+OCO-2 retrievals (blue dots) of temperature at 607, 790 and 972 mb (left column) and associated posterior random errors (right column).

https://doi.org/10.5194/egusphere-2026-6353
Preprint. Discussion started: 9 November 2026
© Author(s) 2026. CC BY 4.0 License.

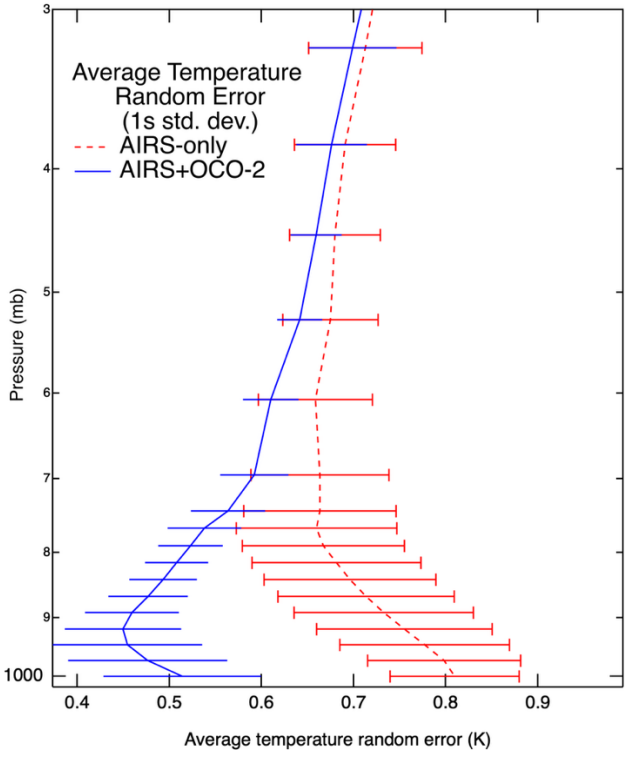


Figure 8: Average random temperature error vs. pressure from retrievals shown in Fig. 7. Error bars are 1σ standard deviations.

Figure 9 shows the water vapor volume mixing ratio retrieval posterior uncertainty as a function of latitude at 607, 790, and 972 mb for both AIRS-only and AIRS+OCO-2. The reduction in posterior error in the mid-troposphere (607 mb) is effectively zero. This due to the limited additional information provided by OCO-2 at higher altitudes. Figure 10 demonstrates that the posterior error is reduced the most at the pressure levels closest to the surface.

https://doi.org/10.5194/egusphere-2026-6353
Preprint. Discussion started: 9 November 2026
© Author(s) 2026. CC BY 4.0 License.

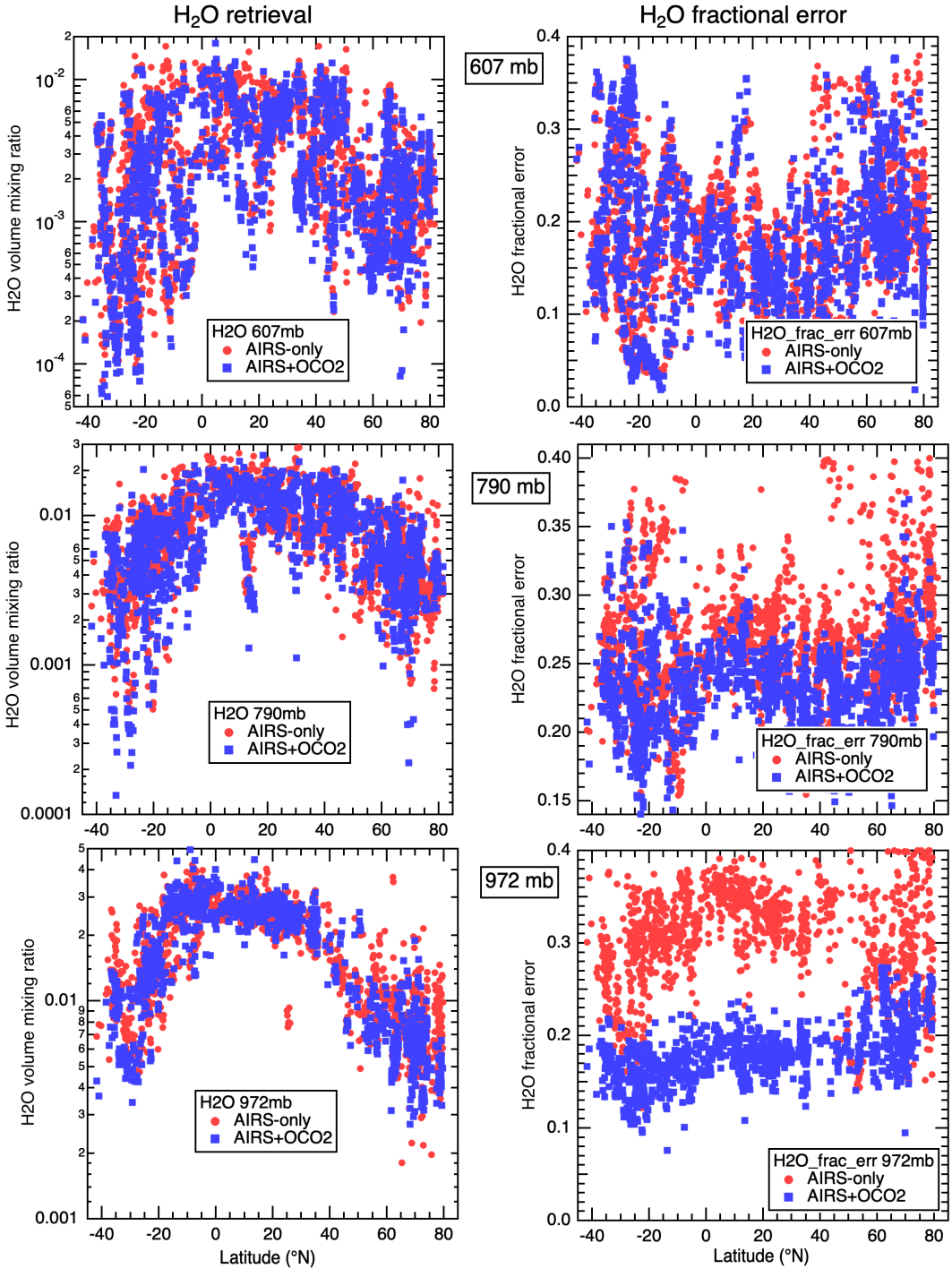


Figure 9: Latitudinal comparison of AIRS-only (red dots) and AIRS+OCO-2 retrievals (blue dots) of water vapor volume mixing ratio at 607, 790 and 972 mb (left column) and associated random fractional errors (right column). Note that the water vapor volume mixing ratio are on a logarithmic scale, while the errors are on a linear scale.

https://doi.org/10.5194/egusphere-2026-6353
Preprint. Discussion started: 9 November 2026
© Author(s) 2026. CC BY 4.0 License.

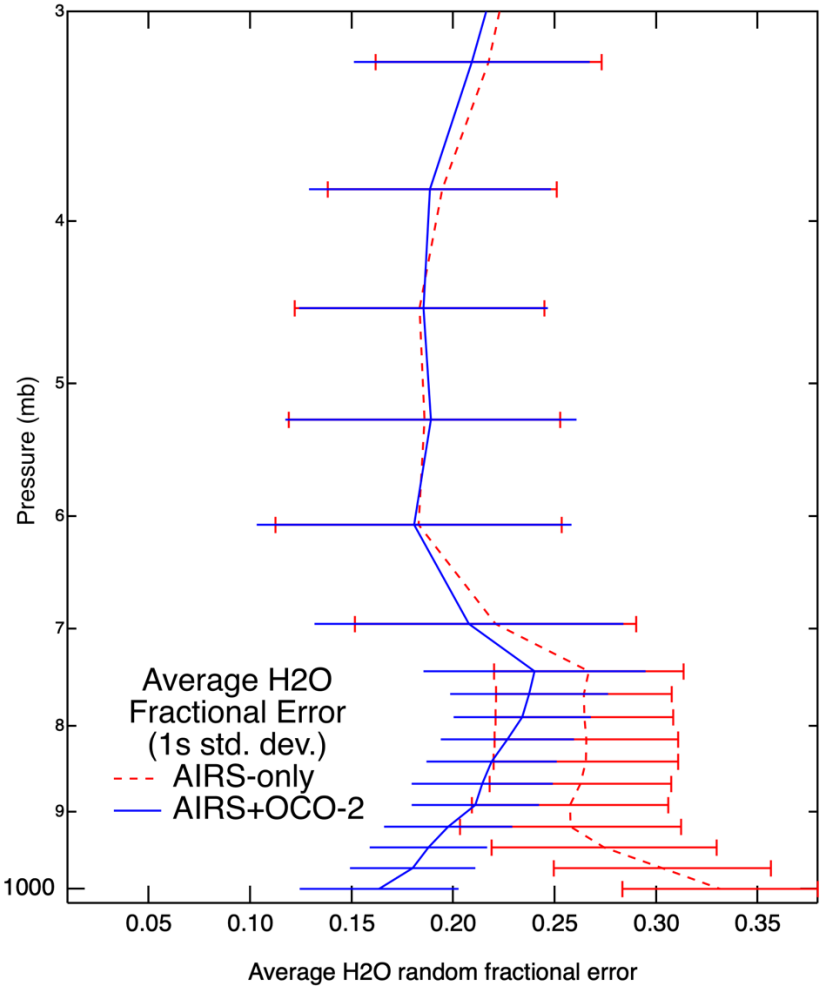


Figure 10: Average random water vapor fractional error vs. pressure from retrievals shown in Fig. 9. Error bars are 1σ standard deviations.

5. Comparison against coincident radiosondes

We compared AIRS-only and AIRS+OCO-2 temperature and water vapor retrievals to Integrated Global Radiosonde Archive (IGRA) radiosondes (Durre et al., 2006) over Europe for the month of July 2017. Sonde launches were within 1 hour and 50 km of the AIRS overpass (for AIRS-only retrievals) and of the OCO-2 overpass for AIRS+OCO-2 retrievals; 29 unique sondes were matched to successful retrievals, with 26 having data at 918 mb. Figure 11 shows the sonde locations, with the numbers indicting the number of days where successful retrievals were made, and the coloring indicating the total number of matchups at that site at 918 mb. The collocations are limited to Europe because of the overpass time of OCO-2/AIRS, typical sonde launch times (0 and 12 UTC), and locations where sondes are launched. As retrievals are made under clear or nearly clear conditions, the number of matchups to a particular sonde can vary widely. Simply averaging biases can introduce significant

https://doi.org/10.5194/egusphere-2026-6353
Preprint. Discussion started: 9 November 2026
© Author(s) 2026. CC BY 4.0 License.

sampling error. We therefore take a "median-of-the-medians" approach to compare AIRS-only retrievals, AIRS+OCO-2 retrievals, and the a priori against the sondes. For the ensemble of a priori and QC-passed retrievals for a single sonde, we calculate the median temperature bias, and fractional bias in H_2O (e.g., [retrieval – sonde]/sonde). From the ensemble of median biases thus calculated, we calculate the "global" median. We also report the interquartile ranges (IQR), that is, the differences between the 75th and 25th percentiles of the results.

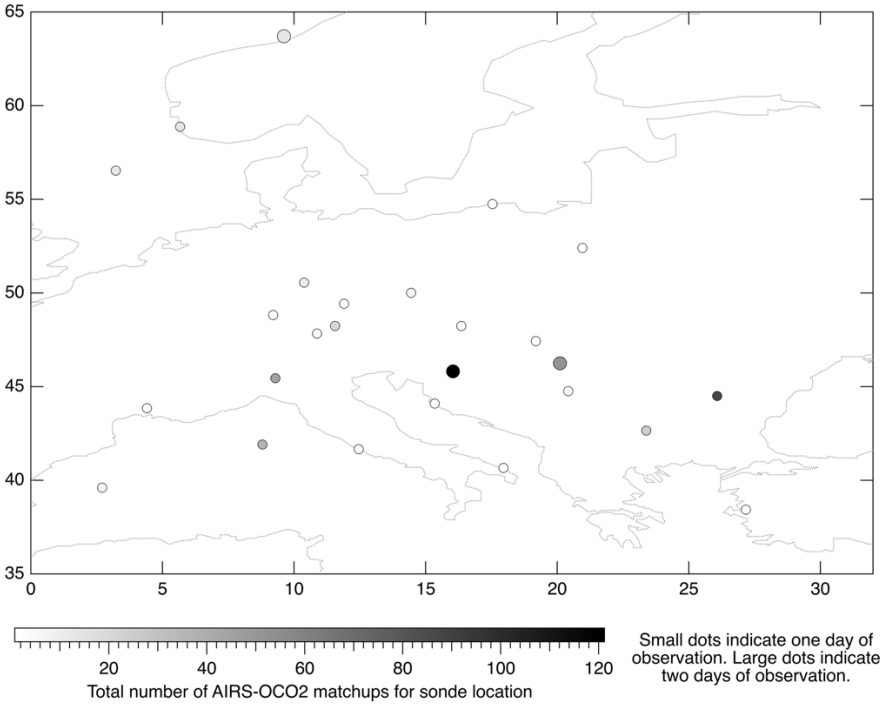


Figure 11: Locations of coincident radiosonde profiles, AIRS-only and AIRS+OCO-2 retrievals for July 2017. Numbers indicate number of sondes for which coincident retrievals at 918 mb could be made during the month, while the color scale indicates the number of successful retrievals for each location.

Figure 12 shows the global median bias against sondes for temperature retrievals and a priori. The a priori tends to be better than both AIRS-only and AIRS+OCO-2 throughout the atmosphere at altitudes above ~800 mb. The AIRS-only retrieval shows a near constant bias of ~0.3 K from the surface to ~400 mb, while AIRS+OCO-2 shows a high bias of ~0.75 K at 900 mb, and a negative bias of ~ -0.7 K at 700 mb. Both AIRS-only and AIRS+OCO-2 show similar low biases at ~250 mb, but we note that almost all of the retrieval information at this pressure is from AIRS. Bias improvements over the prior are seen at the lowest regions with pressures greater than 900 mb, with AIRS-only about 0.5 K, and AIRS+OCO-2 at about 0.75 K above the sonde result. Except at the very highest pressure, the a priori tends to have lower IQRs than either AIRS-only and AIRS+OCO-2.

https://doi.org/10.5194/egusphere-2026-6353
Preprint. Discussion started: 9 November 2026
© Author(s) 2026. CC BY 4.0 License.

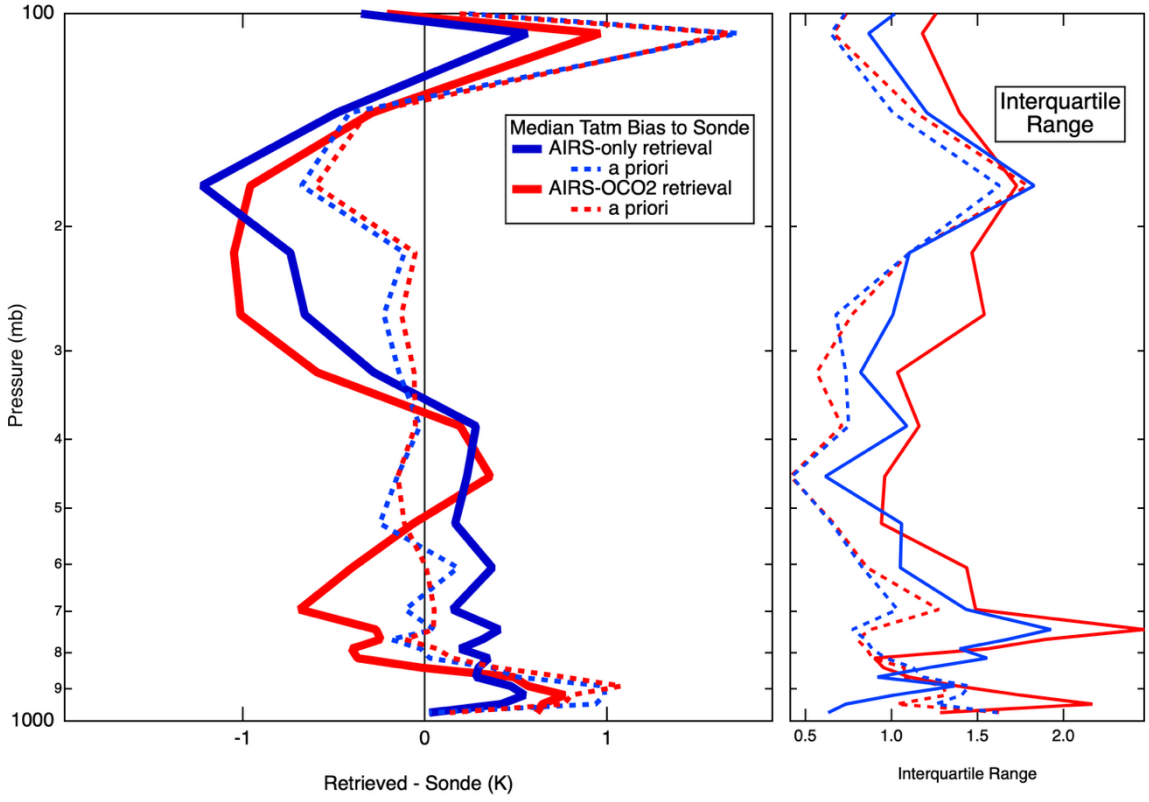


Figure 12: "Median of the Medians" temperature bias and interquartile range of AIRS-only and AIRS+OCO-2 retrievals for locations shown in Fig. 11.

Figure 13 shows the IGRA comparison results for water vapor. The AIRS-only and AIRS+OCO-2 retrieval improve upon the a priori at ~350 mb, however the a priori shows lower biases from ~600 mb to the surface. However, here the addition of OCO-2 to AIRS produces a notably lower bias compared to AIRS-only at pressures greater than ~800 mb, with water vapor within ~10% of the sonde, and produces an IQR comparable to the a priori.

https://doi.org/10.5194/egusphere-2026-6353
Preprint. Discussion started: 9 November 2026
© Author(s) 2026. CC BY 4.0 License.

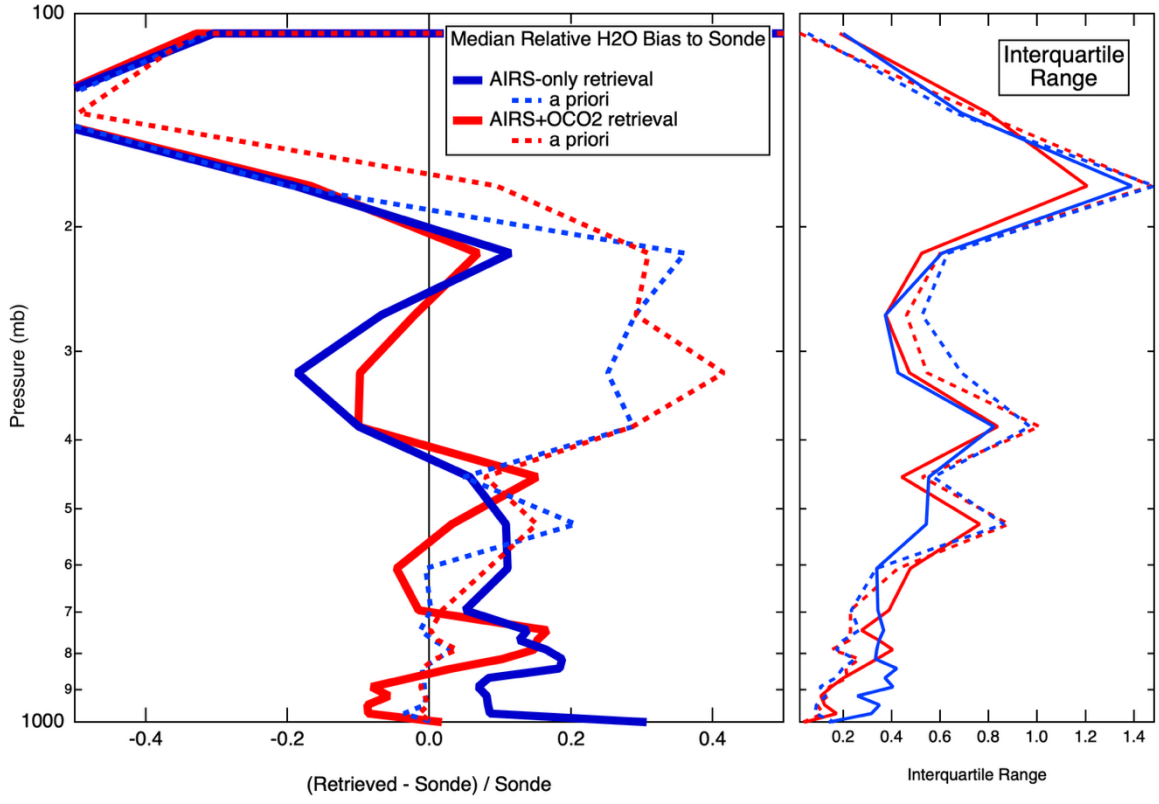


Figure 13: "Median of the Medians" water vapor bias and interquartile range of AIRS-only and AIRS+OCO-2 retrievals for locations shown in Fig. 11.

305

6. Discussion

We have combined thermal infrared spectra from AIRS with near-infrared spectra from OCO-2 in a joint retrieval for daytime temperature and water profiles from the upper troposphere down to the planetary boundary layer. Results show substantial increases in information content and reduced random error over AIRS-only retrieval for pressure layers in or near the PBL, for
310 clear or near-clear scenes over land and ocean glint. Compared to coincident radiosonde results over Europe, median temperature biases are less than the forecast a priori in the PBL at pressures greater than 900 mb but tend to be higher at lower pressures. Water vapor biases in the PBL are lower for the joint AIRS+OCO-2 retrieval than AIRS-alone but are slightly worse than the a priori at pressures greater than 900 mb.

Improvements in this retrieval scheme are obviously needed. First, while noting that the validation of retrievals is quite limited
315 in time and region, both the AIRS-only and AIRS+OCO-2 retrievals show significant systematic errors compared to sondes; how these biases are distributed as spectroscopic or algorithmic origin in the forward modelling of the two instruments, or algorithmic in the retrieval needs to be further studied.

https://doi.org/10.5194/egusphere-2026-6353
Preprint. Discussion started: 9 November 2026
© Author(s) 2026. CC BY 4.0 License.

Second, we have not addressed the key issue of vertical resolution in the boundary layer. As earlier noted, the vertical resolution of thermal-infrared water retrieval in the PBL (even if constrained by a total water column from the near-infrared) will depend in part on the vertical thermal gradient. We do not claim that the vertical resolution of this method will reach the observational goal of ~1km in the PBL for water vapor, as indicated in Section 8.1 of Teixeira et al. (2021). The pressure layering of the TIR and NIR forward models need to match, but the fixed-pressure layering of the SARTA TIR forward model for AIRS may be (currently) too coarse to fully capture and quantify the achievable resolution of the AIRS instrument in ideal conditions. (Due to resource limitations, we could not complete and validate layering modifications to SARTA.) As SARTA is well "tuned" to AIRS (Strow et al., 2006), and used for further studies, modifications in the lower atmosphere layering to retrieve with a higher vertical resolution in the thermal infrared may be needed.

Third, significant increases in the forward-modelling speed for OCO-2 would be necessary to make the process described feasible for routine retrievals from these programs of records; recent progress has been made using Gaussian process regression (Lamminpää et al., 2025). However, here we used the full 1.6 and 2.0 μm bands of OCO-2 in this effort; future development could need only a subset of the OCO-2 channels, shortening the processing time, while still taking advantage of OCO-2 operational XCO_2 retrievals to screen out cloudy scenes.

As summarized in Section 10 of Teixeira et al. (2021), global monitoring of the PBL using the hyperspectral infrared requires both a high horizontal resolution (~1 km) and at least 4-times daily sampling to adequately observe temporal change. Looking forward, a co-boresighted instrument, combining the thermal infrared and the near infrared, may only need a few key channels in the NIR to effectively constrain the PBL temperature and total water column, in a similar way to how, say, MODIS uses NIR channels to retrieve the water column (e.g., Gao and Kaufman, 2003).

Code and data availability

In progress.

Author contributions

FWI and RRN developed the joint retrieval, with FWI concentrating on the AIRS contribution, and RRN concentrating on the OCO-2 contribution. JM developed and de-bugged linkages to the OCO-2 ReFRACTOR code. CH made refinements to the AIRS SARTA forward model. RCW assisted with information content analysis. SW collated and developed validation radiosonde data for comparisons. FWI prepared this manuscript with contributions from all co-authors.

Competing interests

The authors declare no competing interests.

https://doi.org/10.5194/egusphere-2026-6353
Preprint. Discussion started: 9 November 2026
© Author(s) 2026. CC BY 4.0 License.



Disclaimer

Copernicus Publications adds a standard disclaimer: "Copernicus Publications remains neutral with regard to jurisdictional claims made in the text, published maps, institutional affiliations, or any other geographical representation in this paper. While Copernicus Publications makes every effort to include appropriate place names, the final responsibility lies with the authors. Views expressed in the text are those of the authors and do not necessarily reflect the views of the publisher."
Please feel free to add disclaimer text at your choice, if applicable.

Acknowledgements

For their assistance and support, we thank Sergio DeSouza-Machado, Eric Fetzer, Bjorn Lambrigtsen, Amin Nehrir, Mathias Schreier, Larrabee Strow, Joao Texeira, Qing Yue, and in fond memory, Yuk L. Yung. Research was performed at the Jet Propulsion Laboratory, California Institute of Technology under contract to the National Aeronautics and Space Administration.

Financial support

The work was funded through NASA solicitation NNH21ZDA001N (A.45: Decadal Survey Incubation).

References

Aumann, H. H., Chahine, M. T., Gautier, C., Goldberg, M. D., Kalnay, E., McMillin, L. M., Revercomb, H., Rosenkranz, P. W., Smith, W. L., Staelin, D. H., Strow, L. L., and Susskind, J.: AIRS/AMSU/HSB on the Aqua mission: design, science objectives, data products, and processing systems, IEEE T. Geosci. Remote, 41, 253–264, https://doi.org/10.1109/TGRS.2002.80835, 2003.

Basilio, R., Bennett, M. W., Eldering, A., Lawson, P. R., and Rosenberg, R. A.: Orbiting Carbon Observatory-3 (OCO-3), remote sensing from the International Space Station (ISS), Proc. of SPIE Vol. 11151, Sensors, Systems, and Next-Generation Satellites XXIII, 1115109, https://doi.org/10.1117/12.2534996, 2019.

Bowman, K. W., Rodgers, C. D., Kulawik, S. S., Worden, J., Sarkissian, E., Osterman, G., Steck, T., Luo, M., Eldering, A., Shephard, M., Worden, H., Lampel, M., Clough, S., Brown, P., Rinsland, C., Gunson, M., and Beer, R.: Tropospheric Emission Spectrometer: Retrieval method and error analysis, IEEE T. Geosci. Remote, 44, 1297–1307, https://doi.org/10.1109/TGRS.2006.871234, 2006.

Chahine, M. T., Pagano, T. S., Aumann, H. H., Atlas, R., Barnet, C., Blaisdell, J., Chen, L., Divakarla, M., Fetzer, E., J., Goldberg, M., Gautier, C., Granger, S., Hannon, S., Irion, F. W., Kakar, R., Kalnay, E., Lambrigtsen, B. H., Lee, S.-Y., Le Marshall, J., McMillan, W. W., McMillin, L., Olsen, E. T., Revercomb, H., Rosenkranz, P., Smith, W. L., Staelin, D., Strow,

https://doi.org/10.5194/egusphere-2026-6353
Preprint. Discussion started: 9 November 2026
© Author(s) 2026. CC BY 4.0 License.

L. L., Susskind, J., Tobin, D., Wolf, W. and Zhou, L.: AIRS: Improving weather forecasting and providing new data on greenhouse gases, B. Am. Meteorol. Soc., 87(7), 911-926, https://doi.org/10.1175/BAMS-87-7-911, 2006.

Crisp, D., Atlas, R. M., Breon, F.-M., Brown, L. R., Burrows, J. P., Ciais, P., Connor, B. J., Doney, S. C., Fung, I. Y., Jacob, D. J., Miller, C. E., O'Brien, D., Pawson, S., Randerson, J. T., Rayner, P., Salawitch, R. J., Sander, S. P., Sen, B., Stephens, G. L., Tans, P. P., Toon, G. C., Wennberg, P. O., Wofsy, S. C., Yung, Y. L, Kuang, Z., Chudasama, B., Sprague, G., Weiss, B., Pollock, R., Kenyon, D., and Schroll, S.: The Orbiting Carbon Observatory (OCO) mission, Adv. Space. Res. 34, 700-709, https://doi.org/10.1016/j.asr.2003.08.062, 2004.

Crisp, D., Miller, C. E., and DeCola, P. L.: NASA Orbiting Carbon Observatory: Measuring the column averaged carbon dioxide mole fraction from space, J. Appl. Remote Sens., 2, 23508, https://doi.org/10.1117/1.2898457, 2008.

Crisp, D.: "Measuring Atmospheric Carbon Dioxide from Space with the Orbiting Carbon Observatory-2 (OCO-2)" in Earth Observing Systems XX, Proc. of SPIE Vol. 9607, https://doi.org/10.1117/12.2187291, 2015.

Durre, I., Vose, R. S., and Wuertz, D. B.: Overview of the Integrated Global Radiosonde Archive, J. Climate, 19, 53-68, https://doi.org/10.1175/JCLI3594.1, 2006.

Eldering, A., Taylor, T. E., O'Dell, C. W., and Pavlick, R.: The OCO-3 mission: measurement objectives and expected performance based on 1 year of simulated data, Atmos. Meas. Tech., 12, 2341–2370, https://doi:10.5194/amt-12-2341-2019, 2019.

Fu, D., Bowman, K. W., Worden, H. M., Natraj, V., Worden, J. R., Yu, S., Veefkind, P., Aben, I., Landgraf, J., Strow, L., and Han, Y.: High-resolution tropospheric carbon monoxide profiles retrieved from CrIS and TROPOMI, Atmos. Meas. Tech., 9, 2567–2579, https://doi.org/10.5194/amt-9-2567-2016, 2016.

Fu, D., Kulawik, S. S., Miyazaki, K., Bowman, K. W., Worden, J. R., Eldering, A., Livesey, N. J., Teixeira, J., Irion, F. W., Herman, R. L., Osterman, G. B., Liu, X., Levelt, P. F., Thompson, A. M., and Luo, M.: Retrievals of tropospheric ozone profiles from the synergism of AIRS and OMI: methodology and validation, Atmos. Meas. Tech., 11, 5587–5605, https://doi.org/10.5194/amt-11-5587-2018, 2018.

Gao, B.-C., and Kaufman, Y. J.: Water vapor retrievals using Moderate Resolution Imaging Spectroradiometer (MODIS) near-infrared channels, J. Geophys. Res., 108(D13), 4389, https://doi.org/10.1029/2002JD003023, 2003.

Irion, F. W., Kahn, B. H., Schreier, M. M., Fetzer, E. J., Fishbein, E., Fu, D., Kalmus, P., Wilson, R. C., Wong, S., and Yue, Q.: Single-footprint retrievals of temperature, water vapor and cloud properties from AIRS, Atmos. Meas. Tech., 11, 971–995, https://doi.org/10.5194/amt-11-971-2018, 2018.

Irion, F. W., Blaisdell, J. M., Fetzer, E. J., Fishbein, E., Goodman, A., Kahn, B. H., Manning, E., Monarrez, R., Schreier, M. M., Thrastarson, H. Th., Yue, Q.: Algorithm Theoretical Basis Document for the Joint Single Footprint Retrieval Algorithm (JoSFRA), https://doi.org/10.5067/0K06YE0Y8IDS, 2025.

Kuze, A., Suto, H., Nakajima, M., and Hamazaki, T.: Thermal and near infrared sensor for carbon observation Fourier-transform spectrometer on the Greenhouse Gases Observing Satellite for greenhouse gases monitoring, Appl. Optics 48 (35), 6716-6733, https://doi.org/10.1364/AO.48.006716, 2009.

https://doi.org/10.5194/egusphere-2026-6353
Preprint. Discussion started: 9 November 2026
© Author(s) 2026. CC BY 4.0 License.

Lamminpää, O., Susiluoto, J., Hobbs, J., McDuffie, J., Braverman, A., and Owhadi, H.: Forward model emulator for atmospheric radiative transfer using Gaussian processes and cross validation, Atmos. Meas. Tech., 18, 673–694, https://doi.org/10.5194/amt-18-673-2025, 2025.

L'Ecuyer, T. S., and Jiang, J. H.: Touring the atmosphere abord the A-Train, Physics Today, 63, 7, 36-41, https://doi.org/10.1063/1.3653856, 2010.

McDuffie, J., K. Bowman, Jo. Hobbs, V. Natraj, E. Sarkissian, M. T. Mike, and S. Val: Reusable Framework for Retrieval of Atmospheric Composition (ReFRACtor) (Version 1.09), Zenodo [code], https://doi.org/10.5281/zenodo.4019567, 2020.

Miller, C. E., Crisp, D., DeCola, P. L., Olsen, S. C., Randerson, J. T., Michalak, A. M., Alkhaled, A., Rayner, P., Jacob, D. J., Suntharalingham, P., Jones, D. B. A., Denning, A. S., Nicholls, M. E., Doney, S. C., Pawson, S., Boesch, H., Connor, B. J., Fung, I. Y., O'Brien, D., Salawitch, R. J., Sander, S. P., Sen, B., Tans, P., Toon, G. C., Wennberg, P. O., Wofsy, S. C., Yung, Y. L., and Law, R. M.: Precision requirements for space-based XCO_2 data, J. Geophys. Res.-Atmos, 112, D10, D10314, https://doi.org/10.1029/2006JD007659, 2007.

NASEM: Thriving on Our Changing Planet: A Decadal Strategy for Earth Observation from Space, The National Academies Press, Washington, DC., https://doi.org/10.17226/24938, 2018a.

NASEM: The Future of Atmospheric Boundary Layer Observing, Understanding, and Modeling: Proceedings of a Workshop. The National Academies Press, Washington, DC., https://doi.org/10.17226/25138, 2018b.

Nelson, R. R., D. Crisp, L. E. Ott, and C. W. O'Dell: High-accuracy measurements of total column water vapor from the Orbiting Carbon Observatory-2, Geophys. Res. Lett., 43, 12,261–12,269, https://doi.org/10.1002/2016GL071200, 2016.

Nelson, R. R., and O'Dell, C. W.: The impact of improved aerosol priors on near-infrared measurements of carbon dioxide, Atmos. Meas. Tech., 12, 1495–1512, https://doi.org/10.5194/amt-12-1495-2019, 2019.

O'Dell, C. W., Connor, B., Bösch, H., O'Brien, D., Frankenberg, C., Castano, R., Christi, M., Eldering, D., Fisher, B., Gunson, M., McDuffie, J., Miller, C. E., Natraj, V., Oyafuso, F., Polonsky, I., Smyth, M., Taylor, T., Toon, G. C., Wennberg, P. O., and Wunch, D.: The ACOS CO2 retrieval algorithm – Part 1: Description and validation against synthetic observations, Atmos. Meas. Tech., 5, 99–121, https://doi.org/10.5194/amt-5-99-2012, 2012.

O'Dell, C. W., Eldering, A., Wennberg, P. O., Crisp, D., Gunson, M. R., Fisher, B., Frankenberg, C., Kiel, M., Lindqvist, H., Mandrake, L., Merrelli, A., Natraj, V., Nelson, R. R., Osterman, G. B., Payne, V. H., Taylor, T. E., Wunch, D., Drouin, B. J., Oyafuso, F., Chang, A., McDuffie, J., Smyth, M., Baker, D. F., Basu, S., Chevallier, F., Crowell, S. M. R., Feng, L., Palmer, P. I., Dubey, M., García, O. E., Griffith, D. W. T., Hase, F., Iraci, L. T., Kivi, R., Morino, I., Notholt, J., Ohyama, H., Petri, C., Roehl, C. M., Sha, M. K., Strong, K., Sussmann, R., Te, Y., Uchino, O., and Velazco, V. A.: Improved retrievals of carbon dioxide from Orbiting Carbon Observatory-2 with the version 8 ACOS algorithm, Atmos. Meas. Tech., 11, 6539–6576, https://doi.org/10.5194/amt-11-6539-2018, 2018.

Ou, S. S. C., B. H. Kahn, K.-N. Liou, Y. Takano, M. M. Schreier, and Q. Yue: Retrieval of cirrus cloud properties from the Atmospheric Infrared Sounder: The k-coefficient approach using cloud-cleared radiances as input, IEEE T. Geosci. Remote., 51, 1010-1024, https://doi.org/10.1109/TGRS.2012.2205261, 2013.

https://doi.org/10.5194/egusphere-2026-6353
Preprint. Discussion started: 9 November 2026
© Author(s) 2026. CC BY 4.0 License.

Platnick, S., King, M. D., Ackerman, S. A., Menzel, W. P., Baum, B. A., Riédi, J. C., and Frey, R. A.: The MODIS cloud products: Algorithms and examples From Terra, IEEE T. Geosci. Remote, 41, 459–473, https://doi.org/10.1109/TGRS.2002.808301, 2003.

Platnick, S., K. G. Meyer, M. D. King, G. Wind, N. Amarasinghe, and B. Marchant: The MODIS Cloud Optical and Microphysical Products: Collection 6 Updates and Examples From Terra and Aqua, IEEE Trans. Geosci. Remote Sen., 55(1), 502-525, https://doi.org/10.1109/TGRS.2016.2610522, 2017.

Rodgers, C. D.: Inverse Methods for Atmospheric Sounding: Theory and Practice, World Scientific Publishing, Singapore, https://library.wmo.int/idurl/4/36084, 2000.

Seeman, S. W., Borbas, E. E., Knuteson, R. O, Stephenson, G. R., and Huang, H.-L.: Development of a Global Infrared Land Surface Emissivity Database for Application to Clear Sky Sounding Retrievals from Multispectral Satellite Radiance Measurements, J. Appl. Met. Clim., 47, 108-123, https://doi.org/10.1175/2007JAMC1590.1, 2008.

Strow, L. L., S. E. Hannon, S. DeSouza-Machado, H. E. Motteler, and D. Tobin: An Overview of the AIRS radiative transfer model, IEEE T. Geosci. Remote., 41, 303-313, https://doi.org/10.1109/TGRS.2002.808244, 2003.

Strow, L. L., Hannon, S. E., De Souza-Machado, S., Motteler, H. E. and Tobin, D. C.: Validation of the Atmospheric Infrared Sounder radiative transfer algorithm, J. Geophys. Res., 111, D09S06, https://doi:10.1029/2005JD006146, 2006.

Susskind, J., Barnet, C. D., and Blaisdell, J. M.: Retrieval of atmospheric and surface parameters from AIRS/AMSU/HSB data in the presence of clouds, IEEE T. Geosci. Remote, 41, 390–409, https://doi.org/10.1109/TGRS.2002.808236, 2003.

Taylor, T. E., O'Dell, C. W., Frankenberg, C., Partain, P. T., Cronk, H. Q., Savtchenko, A., Nelson, R. R., Rosenthal, E. J., Chang, A. Y., Fisher, B., Osterman, G. B., Pollock, R. H., Crisp, D., Eldering, A., and Gunson, M. R.: Orbiting Carbon Observatory-2 (OCO-2) cloud screening algorithms: validation against collocated MODIS and CALIOP data, Atmos. Meas. Tech., 9, 973–989, https://doi.org/10.5194/amt-9-973-2016, 2016.

Teixeira, J., J. R. Piepmeier, A. R. Nehrir, C. O. Ao, S. S. Chen, C. A. Clayson, A. M. Fridlind, M. Lebsock, W. McCarty, H. Salmun, J. A. Santanello, D. D. Turner, Z. Wang, and X. Zeng: Toward a Global Planetary Boundary Layer Observing System: The NASA PBL Incubation Study Team Report, available at https://science.nasa.gov/earth-science/decadal-surveys/decadal-pbl/, 2021.

van Delst, P.: JCSDA infrared sea surface emissivity model, in Proceedings of the 13th International TOVS study conference, Sainte-Adèle, Québec, Canada, 2003, available at https://itwg.ssec.wisc.edu/wordpress/wp-content/uploads/2023/05/4_2_vandelst_paper_itsc13.pdf.